Soft Matter

PAPER

View Article Online
View Journal | View Issue

Cite this: *Soft Matter*, 2025, **21**, 7860

Diffusive probe penetration for characterization of diffusion-governing length scales in amphiphilic PEG–PCL co-networks

Sebastian Seitel,[a] Nico Perez Lopez,[a] Stephanie Ihmann,[bc] Frank Böhme[b] and Sebastian Seiffert*[a]

We investigate the penetrative probe diffusion in a model amphiphilic polymer co-network (APCN) synthesized *via* a hetero-complementary coupling reaction between 2-(4-nitrophenyl)-benzoxazinone-terminated tetra-poly(ε-caprolactone) (t-PCL) and amino-terminated tetra-poly(ethylene glycol) (t-PEG) using isorefractive dynamic light scattering (DLS). We employ spherical silver nanoparticles (AgNPs) and esterified dextrans of varying molecular weights in the APCN swollen in toluene to get insights about the diffusion-governing length scales, namely the correlation length and the hydrodynamic screening length of the network. The diffusion data are analyzed using hydrodynamic and obstruction models, with the hydrodynamic model proving more suitable for such networks. Our results reveal scaling laws for the correlation length as a function of the polymer volume fraction, matching previous theoretical simulations and experimental findings, alongside the determination of the hydrodynamic screening length, marking the transition from the Rouse to the Zimm regime. Additionally, we demonstrate how structural length scales evolve with swelling, offering more profound insights into the structure–property relationships of APCNs. Comparative diffusion measurements in non-crosslinked t-PEG/t-PCL solutions reveal that network crosslinking significantly affects both the characteristic length scales and the scaling behavior of diffusion.

Received 19th June 2025,
Accepted 18th September 2025

DOI: 10.1039/d5sm00629e

rsc.li/soft-matter-journal

Introduction

Amphiphilic polymer co-networks (APCN) comprise both hydrophobic and hydrophilic components that exhibit phase co-continuity, rendering APCN properties unique. They swell in both water and organic solvents, whereby the surrounding medium strongly influences the underlying network structure of the gels.[1] For this reason, these materials show environmentally sensitive viscoelasticity and selective permeability of both hydrophilic and hydrophobic substances, making them most commonly used for soft contact lenses.[2] Furthermore, they are excellent candidates for use as membranes,[3,4] drug delivery systems,[5,6] tissue engineering,[6,7] and matrices for gel or solid polymer electrolytes.[8,9] Recent advances have further improved APCN mechanical robustness and functionality. For example, peptide blocks combined with cellulose nanocrystals enhance strength while preserving swelling behavior,[10] amphiphilic microcapsules fabricated *via* microfluidics enable selective permeability for drug delivery and microreactors,[11] and dynamic covalent APCNs exhibit self-healing and stretchability suitable for flexible electrolytes.[9] New synthetic routes for attaching peptides to tetra-PEG stars yield well-defined functional materials,[12] while studies on thermal properties in phase-separated APCNs inform temperature-responsive design.[13] Moreover, nanophase-separated morphologies with stable bicontinuous domains allow for tunable swelling and optical transparency, expanding the design possibilities for APCN-based materials.[14]

The transport of probes through APCNs is essential for many applications. Swollen polymer networks allow small, mesoscopic, and even large, flexible substances to diffuse through the network mesh architecture, acting as an obstructing feature.[15] Consequently, the mesh size of a swollen network is a key parameter that describes how freely a probe of a given size can diffuse within the network. For example, immunoisolation membranes show that APCNs have significant potential due to their size selectivity, which arises from the mesh size of the polymer network and the dimensions of the nanochannels formed by the hydrophilic domains. This leads to precise, adjustable size selectivity that allows the permeation of small

[a] *Department of Chemistry, Johannes Gutenberg University Mainz, 55128 Mainz, Germany. E-mail: sebastian.seiffert@uni-mainz.de*
[b] *Leibniz-Institut für Polymerforschung, 01069 Dresden, Germany*
[c] *Organic Chemistry of Polymers, Technical University Dresden, 01062 Dresden, Germany*

molecules such as glucose, insulin, ions, and nutrients, while simultaneously creating an impassable barrier to large proteins, antibodies, and cells.[16] In this context, Tobis *et al.* used an APCN from poly((*R*),(*S*)-*N*-(1-hydroxy-butan-2-yl)acrylamide) and polydimethylsiloxane to create chiral separation membranes with precise mesh size.[4]

To rationally tailor these and other applications, a profound knowledge of the interplay of diffusion-governing microstructural length scales and network composition is essential. As a result, accurate characterization and a clear understanding of the mesh architecture and the diffusion-governing length scales of APCNs are crucial. One such parameter often referred to is the average molecular weight between crosslinks, which was first estimated by Flory and Rehner[17] with their model describing the isotropic swelling of crosslinked rubber. Canal and Peppas used this to calculate the average distance between crosslinks, often called the ''mesh size''.[18] However, the mesh size in polymer gels is not a single, well-defined length but has been rather variously interpreted, including the correlation blob from scattering experiments[19,20] and the elastic blob from rheological measurements.[19,21] To estimate the mesh size, the blob concept introduced by de Gennes is often used, with the de Gennes blob being the correlation blob characterized by the correlation length ξ of polymer chains in a crowded system.[19] For semi-dilute solutions, the correlation length marks the transition from single-chain dominated behavior (dilute-like) at short length scales to many-chain (melt-like) statistics at long length scales.[22]

Another diffusion-governing length scale is the hydrodynamic screening length. Hydrodynamic screening describes how the presence of polymers alters the velocity field from a point force in a fluid. While in a pure solvent, the flow decays weakly over long distances, in polymer solutions, it decays more strongly beyond a characteristic length, the so-called hydrodynamic screening length ξ_H, due to an increased macroscopic viscosity. Hydrodynamic interactions dominate on length scales shorter than ξ_H, and on length scales larger than ξ_H, hydrodynamic interactions are screened by surrounding chains. Consequently, the hydrodynamic screening length indicates a transition from Zimm-type dynamics to Rouse-type dynamics.[23] Therefore, ξ_H is expected to be close to the size of a correlation blob ξ_c in a polymer solution, giving $\xi \approx \xi_H$.[22]

In contrast to these idealized pictures, most gels exhibit a wide distribution of strand lengths between crosslinks, especially when possessing non-ideal network structures.[24] Consequently, it is challenging to determine precise values for microstructural length scales such as the correlation length and the hydrodynamic screening length. Still, accurate knowledge of these length scales is crucial for establishing reliable structure–property relationships and developing applications that require well-defined network architectures. Therefore, the use of model networks with a defined starting structure and just few defects is advantageous for investigating such relations.

Sakai *et al.*[25] popularized a powerful approach using hetero-complementary coupling of tetra-armed polyethylene glycol (t-PEG) to obtain model networks with minimal network defects.[26] Recently, Bunk *et al.*[27] utilized this approach to yield a model APCN by hetero-complementary coupling reaction between amine-functionalized t-PEG and 2-(4-nitrophenyl)-benzoxazinone-terminated tetra-armed poly(ε-caprolactone) (t-PCL). Its reaction and gelation kinetics have been investigated using NMR spectroscopy and computer simulations. Additionally, Flory–Huggins interaction parameters have been estimated for the two star polymers, revealing toluene, chloroform, and THF as co-solvents. Multiple quantum NMR results indicate that the APCN possesses a near model-like structure with just a small fraction of pending arms,[27] despite an enhanced formation of double-links as compared to the work by Sakai *et al.*,[25] rendering it suitable as a reference system for further research. Fribiczer *et al.* studied the impact of swelling in co-solvent and selective solvents on the mechanical properties of the APCN with rheology and AFM.[28] Löser *et al.* studied the structure of the APCN in selective and co-solvent using small-angle X-ray scattering, revealing correlation lengths and microphase separation of the PCL in the networks swollen in the selective solvent water, showing cluster sizes independent of the network concentration. Also, they provided an estimate of the hydrodynamic screening length by monitoring the diffusion of polysaccharides and linear polystyrenes with different molecular weights.[29] However, their use of flexible, linear polystyrenes limits the ability to accurately determine the correlation length as a key structural parameter governing diffusion. Due to their conformational flexibility and ability to reptate through the network, these polymers actually do not serve as reliable probes for extracting well-defined microstructural length scales.

To overcome this limitation, it is of great interest to study the diffusion of rigid, ideally hard-sphere colloidal probes to better estimate structural characteristic parameters such as the correlation length ξ and the hydrodynamic screening length ξ_H in the t-PEG/t-PCL APCN, which is key to understanding the microscopic architecture of the network and how it governs macroscopic transport properties. This is crucial not only for fundamental insights into APCNs but also for tailoring their design in applications where controlled diffusion and selective permeability are essential, such as in drug delivery systems, responsive membranes, and nanofiltration technologies.

Various models have been developed to determine the correlation length of a hydrogel based on free volume, hydrodynamic, and obstruction mechanisms, as well as combinations of these. In this work, we focus on the hydrodynamic model by Cukier and the obstruction model. The hydrodynamic model is given as

$$\frac{D}{D_0} = \exp\left(-k \cdot \frac{r}{\xi}\right) = \exp\left(-k_C \cdot r \cdot \Phi^{0.75}\right) \quad (1)$$

with the probe diffusion coefficient D in the hydrogel, the diffusion coefficient D_0 of the probe in pure solvent, the probe radius r, the constant of proportionality k or k_C related to polymer–solvent interactions, the hydrogel's correlation length ξ, and the polymer volume fraction Φ.[30] Recently, Fujiyabu *et al.* studied the diffusion of water in a crosslinked t-PEG hydrogel and proposed a semi-empirical expression with $k \approx 2$,[31] which

is in agreement with findings from Cheng *et al.*[32] Based on polymer chains obstructing the diffusion of probes through the polymer network, leading to an increase in the path length of diffusive transport,[33] an obstructing model was proposed, expressed as[34,35]

$$\frac{D}{D_0} = \exp\left(-\pi\left(\frac{r + r_f}{\xi + 2r_f}\right)^2\right) \quad (2)$$

with the hydrated radius of the polymer chain r_f. The model was based on the Ogston expression for the distribution of spherical spaces between randomly oriented linear fibres.[36] Both models are developed based on a few assumptions, including: (1) the probe is a hard sphere, (2) intermolecular forces of attraction between the probe and the surrounding network polymer chains are negligible, (3) the mesh size of the gel is equivalent to the mesh size of the corresponding polymer solution of the same concentration, and (4) the polymer chains are immobile relative to the diffusion of the probe over the time scale of the transport process.[37] Additionally, for the obstruction model, the distribution of openings between polymer chains can be approximated by a random distribution of straight fibers.[35]

To determine the hydrodynamic screening length of a swollen network, Löser *et al.*[29] proposed a semi-empirical approach, describing the crossover from Zimm to Rouse limit as

$$\frac{D}{D_0} \sim N^{-(1-\nu)} \quad (3)$$

with N being the number of Kuhn segments constituting a polymer chain of the probe and ν being the Flory exponent.

This work aims to determine the key diffusion-governing length scales, specifically the correlation length and the hydrodynamic screening length, in the PEG–PCL model APCN. We utilize spherical silver nanoparticles (AgNPs) with an average diameter of 4 nm, stabilized by a dodecanethiol organic shell, and esterified dextrans of varying molecular weights as probes. First, we examine the diffusion of penetrating probes across a broad range of polymer volume fractions of the APCN to establish scaling relationships of the diffusion-governing length scales derived from the hydrodynamic and/or the obstruction model. To investigate how length scales and scaling relationships change due to hetero-complementary crosslinking of the diffusion-obstructing surrounding PEG–PCL matrix, we use the respective non-crosslinked t-PEG/t-PCL polymer solutions as a reference. We also aim to verify the applicability of these models for describing probe diffusion in model polymer networks in general. Second, we apply the approach proposed by Löser *et al.*[29] to determine the hydrodynamic screening length from the diffusion of dextrans of various molecular weights in the APCN and the respective solutions. By systematically varying the swelling degree of the APCN from the preparation state to the equilibrium swelling degree, we further explore how network swelling influences the underlying length scales. This comprehensive approach aims to establish scaling relationships for correlation and hydrodynamic screening lengths as functions of APCN composition and swelling degree to enable targeted material design.

To carry out our studies, we employ isorefractive dynamic light scattering (DLS) as a non-perturbative technique, taking advantage of the refractive index matching of the PEG–PCL gel and the co-solvent toluene. This renders the network effectively 'invisible' to light scattering, allowing us to study the diffusion of the introduced probes exclusively. Several groups performed isorefractive DLS before, for example, to investigate the polymer self-diffusion of polystyrene in an isorefractive poly(vinyl methyl ether)/toluene matrix[38] or the sol–gel transition of an isorefractive system by monitoring the diffusion of incorporated gold nanoparticles.[39] By applying this method, we significantly simplify the system, thereby enabling a focused investigation of probe diffusion.

Experimental

Materials

Organic silver nanospheres (4 nm) are purchased from CD Bioparticles. Dextran 2.5 kDa, 10 kDa, and 100 kDa are purchased from Carl Roth. Dextran 6 kDa, trifluoroacetic anhydride, and octanoic acid (>99%) are purchased from Sigma Aldrich. Ethanol absolute is purchased from VWR Chemicals. Chloroform (99.5%) is purchased from Titolchimica. Dichloromethane (>99.8%) is purchased from Fisher Chemical. MilliQ water is produced in an in-house Milli-Q system from Merck. All commercially available chemicals are used without further purification.

Synthesis of amino-terminated tetra-arm polyethylene glycol and 2-(4-nitrophenyl)-benzoxazinone-terminated tetra-arm polycaprolactone is performed as published elsewhere.[27] Briefly, starting from commercially available 10 kDa t-PEG-OH, to yield a better leaving group for the following nucleophilic substitution with ammonia to give amino-terminated t-PEG, the terminal hydroxy groups are first reacted with mesyl chloride. 10 kDa t-PCL-OH is synthesized starting from pentaerythritol using ε-caprolactone, which is polymerized by ring-opening polymerization using $Sn(oct)_2$ as a catalyst. Then, t-PCL-OH is converted to 2-(4-nitrophenyl)-benzoxazinone-terminated t-PCL (t-PCL-Ox) by reaction with 2-(4-nitrophenyl)-4-oxo-4*H*-benzo[*d*][1,3]oxazine-7-carboxylic acid chloride, which is synthesized as described earlier.[40]

Synthesis of hydrophobically modified dextran octanoates

We adapt and modify a previously reported procedure from Togo *et al.*[41] for the derivatization of commercially available dextrans. In general, 10 mL of trifluoroacetic anhydride (TFAA) and 10 mL of octanoic acid are combined in a vacuum-dried two-neck round-bottom flask and heated at 50 °C for 10 minutes under an N_2 atmosphere. Next, 0.5 g of dextran is added to the mixture and stirred at 50 °C for two hours. The reaction mixture is poured slowly into a 9 : 1 mixture of ethanol and water and stirred for several minutes. The precipitate is vacuum filtered, redissolved in chloroform or dichloromethane (depending on the dextran's molecular weight), and

reprecipitated in a 9:1 mixture of ethanol and water. The precipitate is again vacuum filtered and dried under vacuum.

Dex257k (colorless solid, 1.31 g, 71% yield), (400 MHz, $CDCl_3$, δ): 5.47 (t, J = 9.6 Hz, 1H), 5.17 (t, J = 9.4 Hz, 1H), 5.04 (d, J = 3.7 Hz, 1H), 4.81 (dt, J = 9.2, 4.4 Hz, 1H), 3.95 (d, J = 10.4 Hz, 1H), 3.46 (d, J = 11.3 Hz, 1H), 2.40–2.14 (m, 6H), 1.63–1.22 (m, 32H), 0.90–0.85 (m, 9H).

Dex23k (colorless solid, 1.42 g, 61% yield), ^{1}H NMR (400 MHz, $CDCl_3$, δ): 5.47 (t, J = 9.8 Hz, 1H), 5.22–5.10 (m, 1H), 5.04 (d, J = 3.7 Hz, 1H), 4.80 (td, J = 9.2, 3.9 Hz, 1H), 4.00–3.86 (m, 1H), 3.72 (d, J = 7.0 Hz, 1H), 3.46 (d, J = 12.0 Hz, 1H), 2.47–2.12 (m, 6H), 1.67–1.17 (m, 32H), 0.87 (td, J = 6.9, 1.7 Hz, 9H).

Dex15k (colorless solid, 1.12 g, 61% yield), ^{1}H NMR (400 MHz, $CDCl_3$, δ): 5.47 (t, J = 9.7 Hz, 1H), 5.17 (t, J = 9.5 Hz, 1H), 5.04 (d, J = 3.5 Hz, 1H), 4.81 (dd, J = 10.1, 3.8 Hz, 1H), 3.95 (d, J = 10.2 Hz, 1H), 3.71 (t, J = 7.0 Hz, 1H), 3.47 (d, J = 11.0 Hz, 1H), 2.42–2.14 (m, 7H), 1.59–1.19 (m, 33H), 0.87 (td, J = 7.0, 1.6 Hz, 9H).

Dex11k (opaque solid to liquid appearance, 0.89 g, 49% yield), ^{1}H NMR (400 MHz, $CDCl_3$, δ): 5.46 (q, J = 8.1 Hz, 1H), 5.25–5.10 (m, 1H), 5.04 (d, J = 3.6 Hz, 1H), 4.86–4.74 (m, 1H), 3.95 (d, J = 9.7 Hz, 1H), 3.46 (d, J = 10.9 Hz, 1H), 2.45–2.11 (m, 6H), 1.67–1.20 (m, 32H), 0.87 (td, J = 7.0, 1.9 Hz, 9H).

Sample preparation for isorefractive dynamic light scattering

All investigated solutions and APCNs at preparation conditions are prepared in cylindrical quartz glass cuvettes (Hellma, diameter: 10 mm). APCNs at equilibrium swelling are created in custom-made cuvettes featuring a removable PTFE base (Fig. S3). Before use, all cuvettes are precleaned with peroxomonosulfuric acid, sodium hydroxide, and water, then rinsed with hot acetone to remove dust. Afterward, the clean cuvettes are transferred to a laminar flow box, where all subsequent sample preparation steps are performed. Furthermore, all additional equipment, such as Eppendorf pipette tips and glass vials, is precleaned in an acetone fountain to remove dust. Toluene is the general solvent for all measurements, while t-PEG and t-PCL are used in an equimolar ratio with respect to the reactive terminal groups. Solutions of t-PCL-Ox or t-PCL-OH are filtered with a Millex FG filter, and t-PEG-NH2 solutions are filtered using a Millex LG filter. Additional Whatman Anotop 0.02 nm syringe filters are used in conjunction with the Millex LG or Millex FG filters to prepare the respective polymer solutions. AgNP solutions are ultrasonicated before use and filtered through combined Millex LCR and FG filters. All dextran solutions are filtered using Millex FG filters. After filtering the respective solutions, they are combined and thoroughly mixed inside the cuvettes according to the compositions listed in Table S2. All gels are allowed to react for 72 hours at room temperature to ensure complete conversion of the heterocomplementary crosslinking reaction.

Dynamic light scattering

Dynamic light scattering (DLS) measurements were performed using an ALV-SP125 goniometer equipped with an ALV/LSE5004 multi-tau correlator and a fiber-coupled ALV/High QE APD avalanche photodiode featuring pseudo-cross correlation. A 632.8 nm He/Ne laser (Thorlabs Inc.) served as the light source. The sample temperature was maintained at 25 °C using a Huber Pilot One thermostat (Peter Huber Kältemaschinenbau AG, Offenburg, Germany).

Size exclusion chromatography

SEC is conducted on a 1260 Infinity GPC/SEC system from Agilent with an RI detector, using the following columns: Shodex pre-column, Shodex OHpak SB 804, Shodex OHpak SB 803, and Shodex OHpak SB 802.5. THF is used as the eluent.

Results and discussion

Synthesis and characterization of probes for diffusion studies

In the first step, we characterize the dextrans and AgNPs in terms of their diffusion behavior in pure toluene. The commercially available spherical AgNPs coated with dodecanethiol are soluble in toluene without further adjustments. However, as commercially available dextrans are insoluble in toluene, we modify dextran 2.5 kDa, 6 kDa, 10 kDa, and 100 kDa by functionalizing the free hydroxyl groups with octanoic acid to tune their solubility by adapting a synthesis by Togo *et al.*[41]

The functionalized dextrans are analyzed using size exclusion chromatography, giving final molecular weights of 257 kDa (PDI = 1.97), 23 kDa (PDI = 1.39), 15 kDa (PDI = 1.23), and 11 kDa (PDI = 1.13) (Fig. S1).

We characterize the diffusion behavior of esterified dextrans and AgNPs in pure toluene using DLS to obtain the necessary reference data for data analysis later. The resulting correlation curves, shown in Fig. 1, are fitted biexponentially to take potential aggregates into account. The first diffusion coefficient is assumed to describe the diffusion of a single AgNP or dextran, respectively. The obtained diffusion coefficients D can be converted into the corresponding hydrodynamic radii

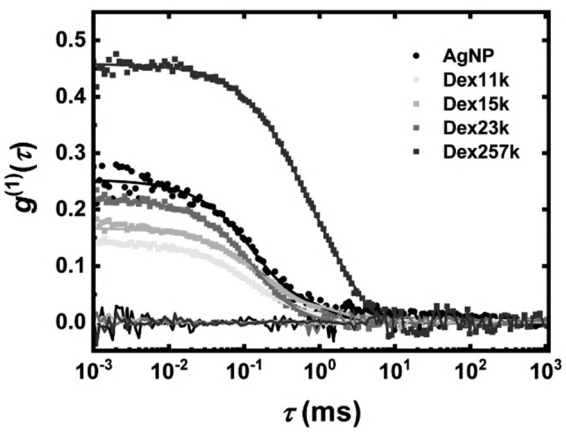

Fig. 1 DLS autocorrelation functions with respective fits and corresponding residual fluctuations around zero for dextrans and AgNPs in toluene at 25 °C measured at a scattering angle of 30°.

R_H using the Stokes–Einstein equation:[22]

$$D = \frac{k_B T}{6\pi\eta R_H} \sim M_w^{-\alpha} \quad (4)$$

with the Boltzmann constant k_B, the temperature T, and the solvent viscosity η. Furthermore, it depends on the molecular weight M_w and can be described by a power law model with scaling exponent α, which depends on the solvent quality, polymer concentration, and polymer conformation.[29]

The determined diffusion coefficients of the probes in toluene and the corresponding hydrodynamic radii are listed in Table 1. All determined hydrodynamic radii appear reasonable. For the esterified dextrans, they increase with increasing molecular weight, while for the AgNPs, they correspond to about half the size of the particles specified by the manufacturer. In the next step, we analyze the functionalized dextrans' diffusion behavior regarding the solvent's quality, which allows us to conclude their molecular conformation. This is essential in understanding and verifying the extent of rigidity as probes for the targeted diffusion studies. For this reason, the hydrodynamic radii R_H are plotted as a function of the respective molecular weights M_w and fitted according to eqn (4) to obtain the scaling exponent $\alpha = 0.36 \pm 0.04$, as shown in Fig. 2.

A comparison with Braeckmans' empirical relation of R_H and M_w for dextrans in aqueous solution ($R_H \sim M_w^{0.53}$)[42] reveals that the obtained exponent for esterified dextrans in toluene is significantly smaller. This is most likely due to the remaining hydrophilic character of the dextran sugar units. To shield those from the rather hydrophobic solvent, the dextrans undergo shrinking, adapting to the form of a compressed globular particle. Thus, it seems reasonable to assume a Zimm-type diffusion behavior of the esterified dextrans in toluene, according to the form $R_H \sim M_w^{\nu}$.[43] In this case, the exponent can be directly transformed into the Flory exponent $\alpha = \nu \approx 1/3$, found in the literature for fully collapsed polymers in a bad solvent.[44] However, since the esterified dextrans are still soluble in toluene, this is quite favorable, as it renders their employment as rigid probe particles for structural investigations of polymer networks very suitable.

Confirming isorefractivity of t-PEG and t-PCL in toluene

Laser light scattering is a powerful nonperturbative method for studying diffusion, dynamic processes, and structural characteristics. Typically, a high refractive index contrast between polymer and solvent is required to generate measurable scattering. In this study, however, we exploit the refractive index matching between PEG, PCL, and toluene, effectively suppressing network-related scattering.

Table 1 Diffusion coefficients of esterified dextrans and AgNPs in toluene and the corresponding hydrodynamic radii

	R_H (nm)	D_0 (10^{-7} cm^2 s^{-1})
Dex257k	9.23 ± 0.50	4.28 ± 0.24
Dex23k	4.20 ± 0.32	9.42 ± 0.68
Dex15k	3.41 ± 0.14	11.57 ± 0.05
Dex11k	2.70 ± 0.22	14.68 ± 1.12
AgNP	2.58 ± 0.33	15.5 ± 0.2

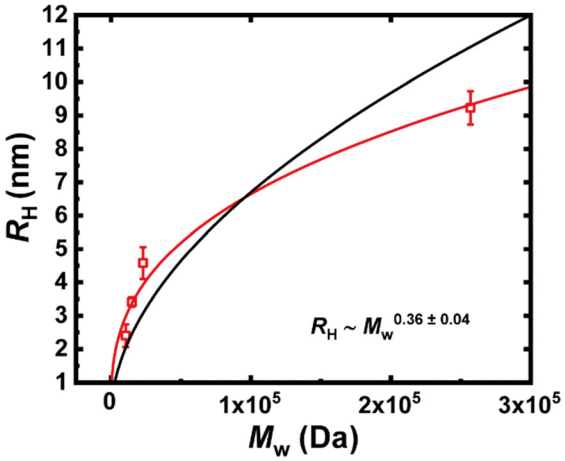

Fig. 2 Hydrodynamic radii of esterified dextrans in toluene plotted against their respective molecular weight. The obtained power law fit (red line) yielded an exponent of 0.36 ± 0.04. For comparison, the power law dependence of dextrans in water, according to Braeckmans',[35] empirical relation, is shown (black line).

This enables us to observe the diffusion of probe particles within the network selectively. To verify the isorefractive conditions, DLS measurements are performed on PEG–PCL APCNs at overlap concentration (70 g L^{-1}) in the preparation state and at swelling equilibrium, as well as on PEG–PCL solutions (70 g L^{-1}). All samples exhibit reduced scattering intensity. For the APCNs in the preparation state, no correlation signal is detected even at a scattering angle of 30°, indicating minimal network contribution to scattering. The swollen APCNs show a weak correlation at 30°, likely due to residual air bubbles introduced during sample transfer (Fig. S3); however, at 50°, correlation is again negligible. In contrast, the PEG–PCL polymer solution requires measurements at 90°, as lower angles still yield noticeable correlation signals, most likely due to the presence of aggregates, particularly of the t-PEG star polymers. The observed effectiveness of refractive index matching is demonstrated in Fig. 3.

Additionally, comparing the scattered intensities normalized to the power of the laser shows roughly the same scattering intensities for the pure solvent and the gel at preparation conditions, swelling equilibrium, or the polymer solution at the respective scattering angle, proving the system's isorefractive behavior. Especially after including the AgNPs, an increased normalized scattering intensity is observed (Fig. S2).

Probe diffusion in APCNs and polymer solutions to determine diffusion-governing length scales

In the next step, we aim to gain insights into the dependency of the probes' diffusion on the APCNs' polymer volume fraction, leading to a more profound understanding of the diffusion-limiting length scales as a function of the polymer volume fraction. For this, we first focus on the diffusion of AgNPs, varying the APCNs polymer volume fraction from 0.75c^* to 3c^*, and from 0.5c^* to 2c^* for the respective t-PEG/t-PCL polymer solution. The obtained correlation curves from isorefractive DLS measurements are displayed in Fig. 4. Other than the

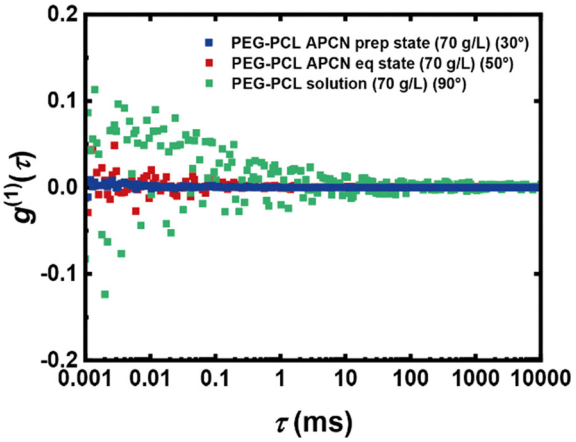

Fig. 3 Dynamic light scattering data obtained for the APCN prepared at overlap concentration at preparation swelling degree at a scattering angle of 30°, at swelling equilibrium at a scattering angle of 50 °C, and for the respective t-PEG/t-PCL solution at a scattering angle of 90°.

correlation curves for the diffusion in a pure solvent, the data herein show a distinctive slow mode. This finding is attributed to the presence of PEG and PCL, which significantly hinder the diffusion. It is also more pronounced for the gel than the respective polymer solutions, which is reasonable due to cross-links in the gel, leading to a more significant hindrance or even trapping of the AgNPs. Both data sets at all concentrations are fitted triexponentially to account for the diffusion of agglomerated, and therefore larger, or trapped particles.

For the APCN in the preparation state, the slowest diffusion coefficients are attributed to nanoparticles effectively immobilized within the network. These trapped particles diffuse so slowly that their characteristic lag times fall outside the temporal resolution of the DLS setup. For this reason, they are excluded from further discussion. The diffusion of a single particle is expected to show the fastest diffusion coefficient. However, a deviation from the decreasing trend of $D_{APCN,1}$ is found because, above the overlap concentration, diffusion appears faster than anticipated (Table S1). This anomaly may result from smaller nanoparticles within the AgNP sample, which diffuse more rapidly, while larger particles experience an increasing hindrance. This interpretation is supported by the amplitudes of the correlation modes: at 1.5c^*, the faster, first mode has a smaller amplitude (0.006) than the slower, second mode (0.011), but with increasing polymer concentration, the amplitude of the faster mode increases (2c^*: 0.018, 3c^*: 0.023), suggesting that these smaller, faster particles become more hindered and detectable within the network. Furthermore, the supplier's certificate confirms particles down to 2 nm diameter, supporting this explanation. Additionally, different diffusion mechanisms may come into play for smaller particles once the polymer correlation length decreases below a critical size, affecting their observed mobility.[45] Thus, $D_{APCN,2}$ is taken as the representative diffusion coefficient for subsequent analysis for all concentrations exceeding the overlap concentration. In the t-PEG/t-PCL polymer solution, the slowest diffusion coefficients are attributed to large agglomerates strongly hindered by the polymer matrix and excluded from further analysis. The primary diffusion mode $D_{sol,1}$ shows a consistent decrease with increasing polymer concentration, while $D_{sol,2}$ is likely arising from larger particles and is also not considered further. For subsequent analysis, the reduced diffusion coefficients D/D_0 are needed. Each reduced diffusion coefficient corresponds to the AgNP diffusion coefficient in solution or in the APCN, normalized to its value in pure toluene. For the APCN, either D_1 or D_2 was used for the respective polymer concentration, as described previously; these are hereafter collectively denoted as D_{prep}. In the case of AgNP diffusion, all reduced diffusion coefficients decrease with increasing polymer volume fraction, as shown in Table 2.

Next, we introduce the esterified dextrans as probes in the t-PEG/t-PCL polymer solution and the corresponding APCN at the overlap concentration. For the APCN, probe diffusion is studied both at preparation conditions and equilibrium swelling degree to gain a deeper understanding of the change of the length scales of the obstructing mesh structure upon change of the swelling degree. Experiments with esterified dextrans were performed exclusively in APCNs prepared at the overlap concentration because the largest dextran, with a hydrodynamic radius of 9.23 ± 0.50 nm, is already roughly three times larger than the expected 'mesh size' of the network at this concentration. Consequently, a significant hindrance to its diffusion is already expected.

The resulting correlation curves are triexponentially fitted to account for the complexity of the hindered dextran diffusion, as shown in Fig. 5.

As in previous analyses, only the fastest diffusion coefficient, describing the diffusion of a single unassociated dextran, is

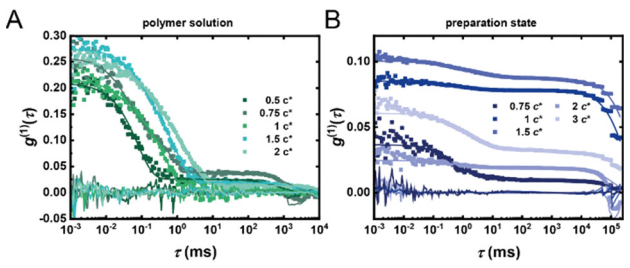

Fig. 4 Dynamic light scattering data obtained for the AgNPs measured in the PEG–PCL polymer solution (A) and APCN (B). Correlation data (squares) and the corresponding fits and residuals (lines) of AgNP diffusion in both samples at various concentrations, measured at 25 °C.

Table 2 Reduced diffusion coefficients obtained for the AgNPs in the polymer solutions and the APCNs at both preparation states at varied polymer volume fractions

ϕ	D_{sol}/D_0	D_{prep}/D_0
0.03	0.53 ± 0.10	—
0.048	0.38 ± 0.05	0.33 ± 0.15
0.06	0.31 ± 0.4	0.21 ± 0.03
0.09	0.21 ± 0.03	0.042 ± 0.013
0.12	0.13 ± 0.02	0.023 ± 0.003
0.18	—	0.006 ± 0.001

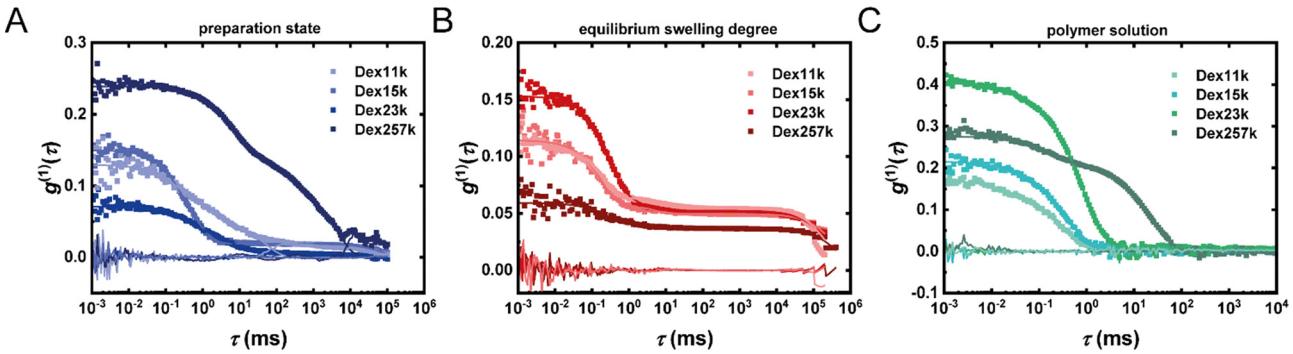

Fig. 5 Autocorrelation functions (rectangles) measured at a scattering angle of 50° for the APCNs and 90° for the polymer solutions with respective fits (solid lines) and corresponding residual fluctuations around zero for dextrans diffusion in (A) APCNs at preparation conditions, (B) at swelling equilibrium and (C) in the respective polymer solutions at overlap concentration.

considered relevant and used for further evaluation. All slower components are excluded from further discussions as they are associated with agglomerates or immobilized species. Overall, the diffusion coefficients exhibit consistent and expected trends. Diffusion is fastest in the polymer solution and decreases with increasing hydrodynamic radius of the probe.

This finding is reasonable given the absence of permanent covalent crosslinks in solution. In contrast, in the APCNs, the dextrans diffusion is more restricted, particularly in the APCN at preparation conditions, compared to the equilibrium-swollen APCN. This is in line with expectations, as the obstructing meshes are anticipated to increase slightly with an increased swelling degree. Consistently, even at the overlap concentration, the measurements reveal a pronounced slow diffusion mode, especially for the largest dextrans. At higher network concentrations, this hindrance would become more severe, further amplifying the slow mode and making it increasingly difficult to accurately extract a single, well-defined diffusion coefficient for each dextran species. Comparative studies at other concentrations were thus not performed, as they would complicate the interpretation due to enhanced hindered mobility.

Again, the reduced diffusion coefficients D/D_0 are calculated for subsequent analysis. As illustrated in Table 3, the values decrease progressively with increasing hydrodynamic radius of the esterified dextrans, aligning with expectations.

Evaluating network correlation length using hydrodynamic and obstruction models

The primary goal of this work is to determine diffusion-governing length scales. In the first step, we analyze the diffusion data of AgNPs to determine the correlation length.

Table 3 Reduced diffusion coefficients obtained for the esterified dextrans in the polymer solutions and the APCNs at both preparation state and swelling equilibrium

	D_{sol}/D_0	D_{prep}/D_0	D_{eq}/D_0
Dex257k	0.32 ± 0.02	0.030 ± 0.004	0.06 ± 0.03
Dex23k	0.63 ± 0.03	0.16 ± 0.02	0.24 ± 0.04
Dex15k	0.77 ± 0.06	0.18 ± 0.05	0.32 ± 0.02
Dex11k	0.91 ± 0.02	0.25 ± 0.02	0.39 ± 0.04

In the diffusion experiments conducted with the AgNPs, we varied the polymer volume fraction of the APCN, so to apply both models, we need to fit the reduced diffusion coefficient against the polymer volume fraction. For both models, a relationship of $\xi^{-1} \sim \Phi^{0.75}$ is assumed for polymer solutions in the semi-dilute regime.[46] However, for gels, a steeper scaling has been reported in literature.[47] Also, for the PEG–PCL APCN, Löser *et al.* determined a scaling exponent of 1.08 ± 0.05 using SAXS.[29] To take this uncertainty about the scaling exponent into account, we substitute the exponent in eqn (1) by an unknown exponent α and change eqn (2) by adding an exponent according to $\xi = \kappa \cdot \Phi^{-\alpha}$ with an unknown proportionality factor κ. With this, the diffusion coefficient of the AgNPs becomes a function of the polymer volume fraction. As a result, fitting of the data according to the hydrodynamic model is done with the following expression:

$$\frac{D}{D_0} = \exp(-k_C \cdot r \cdot \Phi^{\alpha}) \tag{5}$$

For the obstruction model, this leads to:

$$\ln\left(\frac{D}{D_0}\right) = -\pi\left(\frac{\kappa}{r + r_f} \cdot \phi^{-\alpha} + \frac{2r_f}{r + r_f}\right)^{-2} \tag{6}$$

The probe's radius is set equal to the hydrodynamic radius determined from DLS for the AgNPs in toluene, $r = R_H$ = 2.58 nm. Regarding the polymer chain radius, for PEG, a literature value is found to be $r_{f,PEG}$ = 0.23 nm.[34] For PCL, it can be calculated using the following relationship:[34]

$$r_f = \left(\frac{M_m v_s}{l \pi N_A}\right)^{\frac{1}{2}} \tag{7}$$

The value for r_f of the t-PCL unit is determined by assuming that one monomer unit is all-*trans* configurated using a bond angle of 109.5°, which is used to calculate the length of a monomer l (Fig. S4). As a result, eqn (7) gives $r_{f,PCL}$ = 0.25 nm with the monomers molar mass M_m = 114.16 g mol^{-1}, the specific volume of the polymer $v_s = 1/\rho$ = 8.73 × 10^{-7} m^3 g^{-1}, and the length of the monomer unit $l \approx 0.87$ nm and Avogadro's number N_A. Assuming only PEG–PCL crosslinking in the

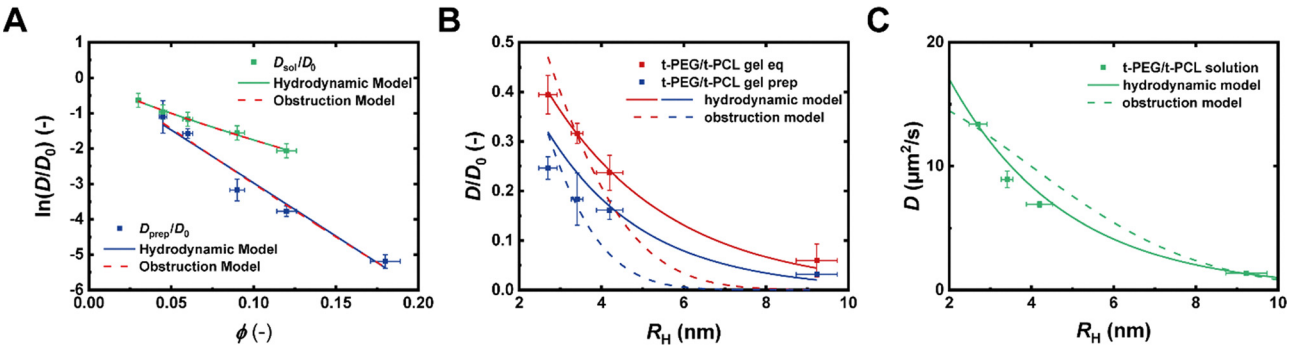

Fig. 6 Diffusion data in the APCNs and the respective polymer solutions are plotted using the hydrodynamic and the obstruction model. (A) Logarithm of the reduced diffusion coefficient of AgNPs plotted against the polymer volume fraction of the APCN and the respective polymer solution. (B) The reduced diffusion coefficients are plotted against the hydrodynamic radii of the respective esterified dextrans in the APCN at preparation conditions and equilibrium swelling. (C) The diffusion coefficients of the dextrans diffusion in the polymer solution at the overlap concentration are plotted against the dextrans hydrodynamic radii.

APCN, the average value r_f = 0.24 nm is used throughout, including the t-PEG/t-PCL polymer solution.

Fig. 6A presents the AgNP diffusion data fitted using the hydrodynamic and obstruction models with unrestricted variables. Although both models yield comparably good fits, the resulting scaling exponents clearly distinguish their validity. In the polymer solution, the hydrodynamic model yields a scaling exponent of 0.81 ± 0.04, closely matching the theoretical prediction of 0.75 for the semidilute regime in a good solvent.[46,48] In contrast, the obstruction model gives a lower exponent of 0.46 ± 0.02, deviating significantly from theory. For the APCN, Löser *et al.* reported a correlation length scaling of 1.08 ± 0.05 with SAXS measurements,[29] consistent with simulations by Scholz *et al.* predicting a scaling near 1.[49] The hydrodynamic model fit yields an exponent of 1.01 ± 0.11, again in excellent agreement with expectations, whereas the obstruction model gives a lower value of 0.61 ± 0.06. These results support the interpretation that the hydrodynamic model is more appropriate for hydrogels composed of flexible chains (*i.e.*, homogenous networks), while the obstruction model better describes systems with rigid or heterogenous structures.[50]

These findings from the AgNP diffusion experiments strongly suggest that the hydrodynamic model provides a more accurate description of probe diffusion in our PEG–PCL APCN than the obstruction model. To validate this conclusion further, we extend our analysis to diffusion experiments using esterified dextrans as soft, deformable probes. This comparison allows us to test whether the superiority of the hydrodynamic model also holds for probes of different rigidity and deformability.

In these experiments, we investigate APCNs prepared at the overlap concentration both in their preparation state and at swelling equilibrium, alongside the corresponding t-PEG/t-PCL polymer solution at the same concentration. Since the varied parameter here is the hydrodynamic radius of the probe, the data can be fitted directly by using either eqn (1) or eqn (2) without further adjustments. Fig. 6B shows the reduced diffusion coefficients for the diffusion of the esterified dextrans in the APCN at preparation conditions and swelling equilibrium, plotted against the respective dextrans hydrodynamic radii and fitted with both models. Again, only the hydrodynamic model accurately reproduces the data, reinforcing the earlier conclusion. The obstruction model would require a much steeper decline in diffusion for larger dextrans than is observed, which is inconsistent with the experimental trend.

Fig. 6C presents the analogous data for the t-PEG/t-PCL polymer solution. As expected, the hydrodynamic model offers a better fit, whereas the obstruction model fails to capture the observed diffusion behavior. The polymer solution is not likely to obstruct the probe's diffusion, but rather increase the solution viscosity, causing increased hydrodynamic drag that slows down the probes. Together, these findings confirm that the hydrodynamic model describes diffusion in both APCNs and corresponding polymer solutions more accurately than the obstruction model for rigid AgNPs and soft dextran probes.

Given its consistent agreement with the experimental data, we employ the hydrodynamic model to extract the correlation length ξ from the reduced diffusion coefficients and the independently determined hydrodynamic radii of the probes. For this purpose, knowing the exponential prefactor k (eqn (1)) is necessary to calculate the correlation length from diffusion experiments with AgNPs. As mentioned earlier, diffusion studies of water in t-PEG model networks by Fujiyabu *et al.*[31] were analyzed using the hydrodynamic model with a proposed prefactor of k = 2, effectively changing the exponent to d_H/ξ, with the hydrodynamic diameter d_H. However, it is noted that water as a solute is at least one order of magnitude smaller than the probes used in this work and much smaller than the expected mesh size of their PEG–PEG network. Furthermore, the difference between a water molecule's hydrodynamic radius and diameter is at a maximum of 0.2 nm, which seems negligible for determining length scales that are roughly one order of magnitude larger. Thus, we adopt an exponential prefactor of k = 1 for our analysis. This assumption is further supported by our finding of k_C = 1.16 ± 0.27 from fitting with the hydrodynamic model. With the exponential prefactor defined, the correlation lengths ξ can now be extracted from the diffusion data using the hydrodynamic model with eqn (1). This enables a quantitative comparison of structure-related length scales across APCNs and polymer solutions.

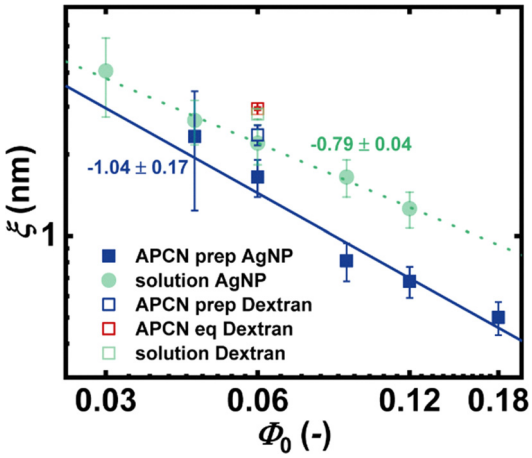

Fig. 7 Values for the correlation lengths determined using the hydrodynamic model and plotted against the corresponding polymer volume fraction at preparation. Fitting of the data with a power-law fit gives a scaling exponent of $\alpha_{APCN} = -1.04 \pm 0.17$ for the APCN at preparation conditions and $\alpha_{Sol} = -0.79 \pm 0.04$ for the t-PEG/t-PCL polymer solutions.

Fig. 7 presents the resulting correlation lengths as a function of the respective polymer volume fraction of the APCN or the polymer solution at preparation Φ_0. All extracted values are within a reasonable size range and agree with Scholz *et al.*'s theoretically determined correlation lengths.[41] As expected, the correlation length decreases with increasing polymer volume fraction. Power-law fitting yields a scaling exponent of -1.04 ± 0.17 for the APCN and -0.79 ± 0.04 for the t-PEG/t-PCL polymer solution, confirming the scaling exponents previously determined from the fits to the reduced diffusion coefficients using the hydrodynamic model. To place these results into context, it is important to consider how the correlation lengths from SAXS, from the theoretical approach from Scholz *et al.*,[49] and from our probe-diffusion study differ in their underlying assumptions. The dynamic correlation length ξ from theoretical studies is obtained by decomposing the total scattering intensity in simulations of star polymer networks into a time-averaged static component and a dynamic part representing liquid-like thermal fluctuations.[49] Experimentally, the correlation length derived from SAXS *via* Ornstein–Zernike analysis similarly reflects these thermal fluctuations,[29] making it conceptually consistent with the theoretically determined dynamic ξ. However, experimental SAXS data do not always easily separate static and dynamic contributions, which may limit the accuracy of SAXS-based correlation lengths.

The correlation length extracted from probe diffusion using the hydrodynamic model is related but different. It represents an effective dynamic 'mesh size' that governs probe mobility and includes additional effects such as probe–polymer interactions, which are not fully captured by scattering techniques. Thus, while comparison of these correlation lengths offers complementary insights, differences in their definitions and sensitivities should be carefully considered. Nevertheless, despite these methodological differences, both the scaling and the absolute values of ξ show good agreement across all approaches.

In the next step, comparing correlation lengths determined from AgNP and esterified dextran diffusion in the same APCN at the overlap concentration and in the preparation state, the dextrans yield an approximately 40% larger value ($\xi_{AgNP} = 1.65 \pm 0.26$ nm; $\xi_{Dex} = 2.36 \pm 0.20$ nm). This result aligns with expectations, since the hydrodynamic model treats the probe as a hard sphere.[50] In contrast, soft, deformable dextrans may experience less hydrodynamic resistance and thus appear to diffuse through a network with a larger effective correlation length. Comparing the values obtained from the diffusion of esterified dextrans in the APCN at the preparation state and the swelling equilibrium reveals an increase of the correlation length by $\sim$25% upon swelling. This reflects the expected loosening of the diffusion-obstructing mesh structure upon solvent uptake, leading to an expanded mesh size. This highlights how swelling systematically alters length scales in the APCN, directly affecting probe mobility.

A similar trend is observed in the polymer solution at overlap concentration: AgNP diffusion yields a correlation length of 2.20 ± 0.37 nm, while dextran diffusion gives a slightly higher value of 2.82 ± 0.12 nm. Both values are in good agreement with the hydrodynamic radii reported for t-PEG and t-PCL ($R_{H,PEG} = 2.4 \pm 0.2$ nm; $R_{H,PCL} = 2.8 \pm 0.2$ nm[27]).

Notably, the correlation lengths in APCNs are systematically smaller than those in the corresponding polymer solutions. This can be attributed to the physical differences between a mobile polymer solution and a crosslinked network. In solutions, polymer chains are free to rearrange around diffusing probes, while the covalent crosslinks in APCNs introduce fixed points of hydrodynamic resistance. In the hydrodynamic model, these fixed chains impose greater frictional drag on the solvent flow around the probe,[50] particularly for probes approaching or exceeding the mesh size. As a result, probe mobility is more strongly hindered in APCNs, leading to lower diffusion coefficients and consequently smaller apparent correlation lengths.

Hydrodynamic screening length from esterified dextrans diffusion

After successfully determining this first diffusion-governing length scale, we now turn to the second key structural parameter, the hydrodynamic screening length. To determine this length, we follow the approach proposed by Löser *et al.*[29] A reduced diffusion coefficient of nearly one is expected for probes smaller than the hydrodynamic screening length, as almost no diffusion hindrance should occur. When the probe's hydrodynamic radius approaches the mesh size, roughly estimated by the hydrodynamic screening length, a crossover regime between free and hindered diffusion emerges. As stated by Löser *et al.*,[29] the resulting diffusion is best described using a combined expression accounting for free diffusion in the Zimm limit and hindered diffusion in the Rouse regime. Their semi-empirical derived relation in eqn (3) can be extended to

$$\frac{D}{D_0} \sim N^{-(1-\nu)} \sim N^{\alpha} \sim M_w^{\alpha} \quad (8)$$

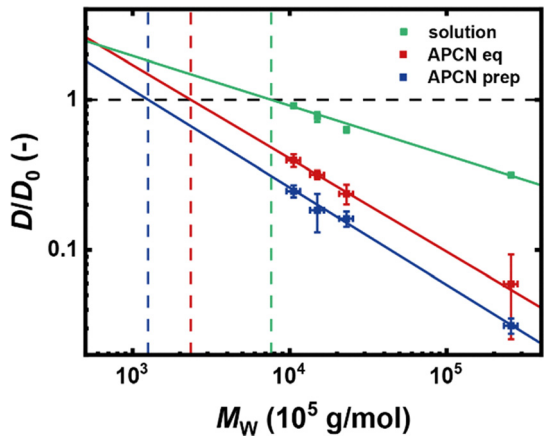

Fig. 8 Reduced diffusion coefficient D/D_0 of dextrans plotted against their respective molecular weight. For small M_w we expect $D/D_0 \approx 1$, while at higher M_w a transition towards $D/D_0 \sim N^{-(1-\nu)}$ is expected. The latter regime is extrapolated towards $D/D_0 \approx 1$ to yield $M_w = 1.26 \pm 0.49$ kDa for the APCN at preparation conditions, $M_w = 2.35 \pm 1.27$ kDa for the APCN at equilibrium swelling degree, and $M_w = 7.21 \pm 5.59$ kDa for the corresponding polymer solution at overlap concentration.

as the number of Kuhn segments N is directly proportional to the probe's molecular weight M_w. Also, with $\nu = 0.36$, this results in a predicted scaling of $D/D_0 \sim M_w^{-0.64}$. Fig. 8 shows the reduced diffusion coefficients of esterified dextrans plotted against their molecular weight and fitted according to eqn (8).

For the APCN, the obtained scaling exponents are $\alpha_{prep} = -0.65 \pm 0.02$ in the preparation state and $\alpha_{eq} = -0.62 \pm 0.03$ at the equilibrium swelling degree. Both values closely match the theoretical expectation, indicating that diffusion in the network follows the predicted crossover behavior. Notably, the swelling degree does not influence the scaling exponents; it only affects the overall diffusion speed of the probes. In contrast, the t-PEG/t-PCL solution yields a scaling exponent of $\alpha_{sol} = -0.33 \pm 0.02$. Although eqn (8) was derived initially assuming that gels and solutions in the semi-dilute regime behave similarly at equal concentration, the absence of crosslinks in the polymer solution leads to a weaker diffusion hindrance. The observed exponent appears to $\alpha = -\nu$, but this interpretation currently lacks theoretical justification.

Further insights are gained by extrapolating the fitted curves to $D/D_0 = 1$, revealing the hydrodynamic screening length, which is comparable to the respective hydrodynamic radius of a hypothetical dextran at this point. Thereby, we obtain $M_w = 1.26 \pm 0.49$ kDa (equivalent to $R_H = \xi_{H,prep} = 1.38 \pm 0.19$ nm) for the APCN at preparation state, $M_w = 2.35 \pm 1.27$ kDa (equivalent to $R_H = \xi_{H,eq} = 1.73 \pm 0.34$ nm) for the APCN at equilibrium swelling degree, and $M_w = 7.21 \pm 5.59$ kDa (equivalent to $R_H = \xi_{H,sol} = 2.65 \pm 0.70$ nm) for the t-PEG/t-PCL polymer solution at overlap concentration. These results confirm the existence of a well-defined hydrodynamic screening length across all systems. As observed for the correlation length, the screening length increases by ~25% upon swelling. It is also noted that the obtained values are roughly twice as large in comparison to the diffusion studies presented by Löser *et al.*[29] ($\xi_{H,eq} = 1.73 \pm 0.34$ nm *vs.* $\xi_{H,eq,Löser} = 0.78 \pm 0.19$ nm), which is most likely due to their use of linear, non-rigid polystyrene tracers, leading to a less hindered diffusion.

Despite identical polymer concentrations, the obtained hydrodynamic screening length for the polymer solution is roughly double that in the APCN at preparation conditions. This highlights the pronounced impact of crosslinks on the hydrodynamic environment. However, the value for $\xi_{H,sol}$ is perfectly in line with expectations as it is in very good agreement with the hydrodynamic radii of t-PEG and t-PCL,[27] as at the overlap concentration, both excluded volume and hydrodynamic interactions should apply over length scales comparable to the size of the entire chain, with $\xi_H \approx \xi \approx R_H$.[22] In contrast, the APCNs show a clear separation of length scales, with the correlation length exceeding the hydrodynamic screening length by a factor of approximately 1.7 at both swelling states, again emphasizing the role of network connectivity in limiting long-range hydrodynamic interactions.

One last important question to address is whether the mobility of the probes is especially affected by the unique structure of the APCN. SAXS measurements by Löser *et al.*,[29] performed on the same network in toluene under identical preparation conditions and concentration range as in our experiments, revealed a homogeneous network structure without microphase separation or any structural characteristics beyond the correlation length. This suggests that the network architecture does not lead to significant phase segregation or large-scale inhomogeneities that would affect probe diffusion. While the amphiphilic nature of the network might intuitively suggest possible localized heterogeneities or probe–network interactions, our data show no evidence of such effects significantly influencing probe mobility. Complementary structural investigations using techniques like light scattering or SANS could further clarify subtle differences, but based on current evidence, the amphiphilic character does not appear to impose measurable restrictions on diffusion behavior.

This structural uniformity is further supported by the solvent environment and polymer–solvent interactions. While interaction parameters determined from viscosity data indicate that in toluene, PCL is better solvated compared to PEG ($\chi_{PCL,toluene} = -0.05$ and $\chi_{PEG,toluene} = 0.38$),[27] toluene remains a good solvent for both polymers. Although this difference could in principle lead to local variations in chain swelling or segmental density, previous work by Bunk *et al.*[27] reported no miscibility issues arising from the use of these two different star polymers in the same network, consistent with the SAXS findings by Löser *et al.*[29] Therefore, the network remains overall homogeneous, and consistently, we observe no indications of specific effects on probe diffusion arising from amphiphilicity.

Conclusion

In this work, model amphiphilic polymer co-networks are prepared by hetero-complementary crosslinking of

amino-terminated t-PEG and benzoxazinone-terminated t-PCL, and their internal microstructure is investigated using diffusive probe penetration studied by isorefractive DLS. To characterize the diffusion-governing length scales of these networks swollen in toluene, we analyze the diffusion of spherical silver nanoparticles (AgNPs) and esterified dextrans of various molecular weights. As expected, probe diffusion gets increasingly hindered with higher polymer volume fractions (in the case of AgNPs) or increasing molecular weight (for dextrans), consistent with a more obstructed network mesh. Across all conditions, the hydrodynamic model provides an excellent fit to the data, yielding correlation lengths in very good agreement with theoretical predictions, in both absolute values and their scaling with polymer concentration.[29,46,49] In contrast, the obstruction model fails to capture the observed diffusion behavior. Furthermore, the hydrodynamic screening length is extracted by analysis of molecular weight-dependent diffusion data of esterified dextran probes. The resulting screening lengths fall within a physically meaningful range, marking the transition from the Zimm to the Rouse regime. Importantly, both the correlation length and the hydrodynamic screening length increase upon swelling from preparation conditions to equilibrium, by approximately 25%, demonstrating that the swelling degree systematically modulates structural and dynamic length scales. A comparison with the corresponding polymer solution at the same concentration further shows that, while hydrodynamic and correlation lengths coincide in solution ($\xi_H \approx \xi \approx R_H$), they decouple in the network due to the presence of crosslinks, following a consistent relationship of $\xi \approx 1.7\xi_H$.

This work characterizes the two key length scales, correlation length and hydrodynamic screening length, that govern probe transport in APCNs. These findings represent an essential step toward a rational understanding and designing APCNs with tailored permeability and transport properties, such as for membrane applications or controlled delivery systems.

While the current study focuses on networks swollen in toluene, a co-solvent, the methodology developed here lays important groundwork for also investigating diffusion in microphase-separating APCNs under selective solvent conditions. In aqueous environments, for example, the PCL blocks collapse into spherical clusters,[29] leading to turbidity that challenges light scattering measurements. To overcome this, diffusion studies could employ non-esterified dextrans labeled with fluorescent dyes, enabling complementary techniques such as fluorescence recovery after photobleaching (FRAP) or fluorescence correlation spectroscopy (FCS) to selectively probe transport within the continuous phase. Such extensions would further deepen our understanding of diffusion processes in complex APCN morphologies relevant to many practical applications.

Conflicts of interest

The authors declare no conflict of interest.

Data availability

All data supporting the findings of this study are included in the article or the attached supplementary information (SI). Supplementary information is available. See DOI: **https://doi.org/10.1039/d5sm00629e**.

Dynamic light scattering DLS autocorrelation functions were fitted using *HDRC*, a custom, lab-specific software for analyzing DLS data. Equivalent fitting procedures can also be performed using commercially available software such as *OriginPro* (OriginLab Corporation). Further data processing and visualization were conducted using *OriginPro*. No additional datasets, software, or code were generated or analyzed during this study.

Acknowledgements

The authors thank the German Research Foundation (DFG) for funding the collaborative Research Unit FOR2811 under Grant No. 397384169, along with project grants 423373052 and 423514254.

Notes and references

1 (*a*) G. Erdodi and J. P. Kennedy, *Prog. Polym. Sci.*, 2006, **31**, 1–18; (*b*) C. S. Patrickios and T. K. Georgiou, *Curr. Opin. Colloid Interface Sci.*, 2003, **8**, 76–85.
2 (*a*) Z. Mutlu, S. Shams Es-Haghi and M. Cakmak, *Adv. Healthcare Mater.*, 2019, **8**, e1801390; (*b*) P. C. Nicolson and J. Vogt, *Biomaterials*, 2001, **22**, 3273–3283.
3 (*a*) K. Schöller, S. Küpfer, L. Baumann, P. M. Hoyer, D. de Courten, R. M. Rossi, A. Vetushka, M. Wolf, N. Bruns and L. J. Scherer, *Adv. Funct. Mater.*, 2014, **24**, 5194–5201; (*b*) G. Erdodi and J. P. Kennedy, *J. Polym. Sci., Part A: Polym. Chem.*, 2005, **43**, 4965–4971.
4 J. Tobis, L. Boch, Y. Thomann and J. C. Tiller, *J. Membr. Sci.*, 2011, **372**, 219–227.
5 (*a*) P. Grossen, D. Witzigmann, S. Sieber and J. Huwyler, *J. Controlled Release*, 2017, **260**, 46–60; (*b*) Y.-Y. Liu, Y.-H. Shao and J. Lü, *Biomaterials*, 2006, **27**, 4016–4024; (*c*) L. Bromberg, M. Temchenko and T. A. Hatton, *Langmuir*, 2002, **18**, 4944–4952; (*d*) M. L. Adams, A. Lavasanifar and G. S. Kwon, *J. Pharm. Sci.*, 2003, **92**, 1343–1355.
6 G. Lin, L. Cosimbescu, N. J. Karin, A. Gutowska and B. J. Tarasevich, *J. Mater. Chem. B*, 2013, **1**, 1249–1255.
7 (*a*) H. Wang, Q. Li, J. Yang, J. Guo, X. Ren, Y. Feng and W. Zhang, *J. Mater. Chem. B*, 2017, **5**, 1408–1422; (*b*) R. Murphy, D. P. Walsh, C. A. Hamilton, S.-A. Cryan, M. in Het Panhuis and A. Heise, *Biomacromolecules*, 2018, **19**, 2691–2699.
8 (*a*) K. R. McLeod and G. N. Tew, *Macromolecules*, 2017, **50**, 8042–8047; (*b*) E. Glynos, C. Pantazidis and G. Sakellariou, *ACS Omega*, 2020, **5**, 2531–2540.
9 D. E. Apostolides, G. Michael, C. S. Patrickios, B. Notredame, Y. Zhang, J.-F. Gohy, S. Prévost, M. Gradzielski, F. A. Jung and C. M. Papadakis, *ACS Appl. Mater. Interfaces*, 2024, **16**, 23813–23825.

10 S. T. R. Velasquez, D. Jang, J. Thomas, P. Grysan, L. T. J. Korley and N. Bruns, *Polym. Chem.*, 2025, **16**, 2618–2628.
11 S. T. R. Velasquez, A. Belluati, E. Tervoort, I. Mattich, B. Hertel, S. Russell, M. G. Gouveia, P. Grysan, C. Mugemana, A. R. Studart and N. Bruns, *Adv. Mater. Technol.*, 2024, **9**, 2400109.
12 D. E. Apostolides, G. Michael, C. S. Patrickios, T. Sakai, I. Kyroglou, M. Kasimatis, H. Iatrou, S. Prévost and M. Gradzielski, *Gels*, 2025, **11**, DOI: 10.3390/gels11050331.
13 A. Petróczy, I. Szanka, L. Bereczki, N. Hegyesi, J. Madarász and B. Iván, *Polymers*, 2025, **17**, DOI: 10.3390/polym17121656.
14 A. Petróczy, I. Szanka, A. Wacha, Z. Varga, Y. Thomann, R. Thomann, R. Mülhaupt, L. Bereczki, N. Hegyesi and B. Iván, *Gels*, 2025, **11**, DOI: 10.3390/gels11050318.
15 K. Saalwächter and S. Seiffert, *Soft Matter*, 2018, **14**, 1976–1991.
16 S. Ulrich, L. F. Boesel and N. Bruns, in *Amphiphilic Polymer Co-networks*, ed. C. S. Patrickios, Royal Society of Chemistry, Cambridge, 2020, pp. 331–363.
17 (*a*) P. J. Flory and J. Rehner, *J. Chem. Phys.*, 1943, **11**, 512–520; (*b*) P. J. Flory and J. Rehner, *J. Chem. Phys.*, 1943, **11**, 521–526; (*c*) P. J. Flory, *J. Chem. Phys.*, 1950, **18**, 108–111.
18 T. Canal and N. A. Peppas, *J. Biomed. Mater. Res.*, 1989, **23**, 1183–1193.
19 P. G. de Gennes, *Scaling Concepts in Polymer Physics*, Cornell University Press, Ithaca, NY, USA, 1979, ch. 3, 5, 7 and 8.
20 H. Oikawa and K. Murakami, *Macromolecules*, 1991, **24**, 1117–1122.
21 T. Sakai, M. Kurakazu, Y. Akagi, M. Shibayama and U. Chung, *Soft Matter*, 2012, **8**, 2730.
22 M. Rubinstein and R. H. Colby, *Polymer Physics*, Oxford University Press, New York, 2003, ch. 8.
23 M. Doi and S. F. Edwards, *The Theory of Polymer Dynamics*, Clarendon Press, Oxford, 1st edn, 1986, pp. 173–174.
24 J. Li and D. J. Mooney, *Nat. Rev. Mater.*, 2016, **1**, 16071.
25 T. Sakai, T. Matsunaga, Y. Yamamoto, C. Ito, R. Yoshida, S. Suzuki, N. Sasaki, M. Shibayama and U. Chung, *Macromolecules*, 2008, **41**, 5379–5384.
26 (*a*) Y. Gu, J. Zhao and J. A. Johnson, *Angew. Chem., Int. Ed.*, 2020, **59**, 5022–5049; (*b*) M. Shibayama, X. Li and T. Sakai, *Colloid Polym. Sci.*, 2019, **297**, 1–12.
27 C. Bunk, L. Löser, N. Fribiczer, H. Komber, L. Jakisch, R. Scholz, B. Voit, S. Seiffert, K. Saalwächter, M. Lang and F. Böhme, *Macromolecules*, 2022, **55**, 6573–6589.
28 N. Fribiczer, K. Hagmann, C. Bunk, F. Böhme, R. von Klitzing and S. Seiffert, *Macro Chem. Phys.*, 2024, **225**(6), 2300389.
29 L. Löser, C. Bunk, R. Scholz, M. Lang, F. Böhme and K. Saalwächter, *Macromolecules*, 2024, **57**, 940–954.
30 R. I. Cukier, *Macromolecules*, 1984, **17**, 252–255.
31 T. Fujiyabu, X. Li, U. Chung and T. Sakai, *Macromolecules*, 2019, **52**, 1923–1929.
32 Y. Cheng, R. K. Prud'homme and J. L. Thomas, *Macromolecules*, 2002, **35**, 8111–8121.
33 B. Amsden, *Polymer*, 2002, **43**, 1623–1630.
34 B. Amsden, *Macromolecules*, 1999, **32**, 874–879.
35 N. A. Hadjiev and B. G. Amsden, *J. Controlled Release*, 2015, **199**, 10–16.
36 A. G. Ogston, *Trans. Faraday Soc.*, 1958, **54**, 1754.
37 B. G. Amsden, *Macromolecules*, 2022, **55**, 8399–8408.
38 J. E. Martin, *Macromolecules*, 1984, **17**, 1279–1283.
39 (*a*) X. Li, N. Watanabe, T. Sakai and M. Shibayama, *Macromolecules*, 2017, **50**, 2916–2922; (*b*) N. Watanabe, X. Li and M. Shibayama, *Macromolecules*, 2017, **50**, 9726–9733.
40 L. Jakisch, M. Garaleh, M. Schäfer, A. Mordvinkin, K. Saalwächter and F. Böhme, *Macro Chem. Phys.*, 2018, **219**, 1700327.
41 A. Togo, Y. Enomoto, A. Takemura and T. Iwata, *J. Wood Sci.*, 2019, **65**, 66.
42 K. Braeckmans, L. Peeters, N. N. Sanders, S. C. de Smedt and J. Demeester, *Biophys. J.*, 2003, **85**, 2240–2252.
43 S. Seiffert, *Physical Chemistry of Polymers*, De Gruyter, Berlin/Boston, 2020, p. 82.
44 S. S. Jang, T. Çağin and W. A. Goddard, *J. Chem. Phys.*, 2003, **119**, 1843–1854.
45 L.-H. Cai, S. Panyukov and M. Rubinstein, *Macromolecules*, 2011, **44**, 7853–7863.
46 P. G. de Gennes, *Macromolecules*, 1976, **9**, 594–598.
47 (*a*) E. Geissler, A.-M. Hecht, S. Mallam, F. Horkay and M. Zrinyi, *Makromol. Chem., Macromol. Symp.*, 1990, **40**, 101–108; (*b*) S. Mallam, F. Horkay, A. M. Hecht, A. R. Rennie and E. Geissler, *Macromolecules*, 1991, **24**, 543–548.
48 R. H. Colby, *Rheol. Acta*, 2010, **49**, 425–442.
49 R. Scholz and M. Lang, *Macromolecules*, 2024, **57**, 2539–2555.
50 B. Amsden, *Macromolecules*, 1998, **31**, 8382–8395.